A One-Dimensional Global-Scaling Erosive Burning Model Informed by Blowing Wall Turbulence

Timothy P. Kibbey[1]
Jacobs, ESSSA Group, Huntsville, AL, 35806

    A derivation of turbulent flow parameters, combined with data from erosive burning test motors and blowing wall tests results in erosive burning model candidates useful in one-dimensional internal ballistics analysis capable of scaling across wide ranges of motor size. The real-time burn rate data comes from three test campaigns of subscale segmented solid rocket motors tested at two facilities. The flow theory admits the important effect of the blowing wall on the turbulent friction coefficient by using blowing wall data to determine the blowing wall friction coefficient. The erosive burning behavior of full-scale motors is now predicted more closely than with other recent models.

Nomenclature

1D	=	one-dimensional
AP	=	ammonium perchlorate
BARF	=	burning anomaly rate factor
B_f	=	blowing parameter
C_{f0}	=	friction coefficient without blowing
C_f	=	friction coefficient with blowing
CFD	=	computational fluid dynamics
CP	=	center perforated propellant grain
D	=	diameter
ETM-3	=	engineering test motor 3
JPL	=	Jet Propulsion Laboratory
k_s	=	equivalent roughness
NMcD	=	new McDonald number
r_e	=	total burn rate including erosive burning
r_0	=	base burn rate
δr_e	=	erosive delta, $r_e - r_0$
RSRM	=	reusable solid rocket motor
RSRMV	=	five-segment reusable solid rocket motor
U_{1D}	=	bulk, average velocity
v_w	=	flow velocity entering at the wall

I. Introduction

Erosive burning, the phenomenon where the burn rate of solid rocket motor propellant is augmented by flow across the surface, has long been studied. This paper makes no attempt to comprehensively review erosive burning models or the data collected in pursuit of them; the interested reader could begin with Landsbaum[1] for a historical summary. Suffice it to say that the search for a way to predict erosive burning in any size motor with formulae cleanly applicable to a typical one-dimensional (1D) ballistics analysis has long been thwarted. Some models were based on testing that failed to adequately simulate the solid rocket motor environment. In most cases, no real-time burn rate measurement was available. Two popular models, even when calibrated to recent motor-like real-time burn rate data obtained by Furfaro[2], are inadequate at modeling erosive burning in the Space Shuttle

---

Reusable Solid Rocket Motor (RSRM), the Space Launch System's Five-Segment RSRM (RSRMV), or the five-segment Engineering Test Motor (ETM)-3.

The difficulty with all attempts to model erosive burning and account for motor scale is how to link the overall flow parameters (scale-related) with the very local burning behavior (non-scale-related). Recent work by McDonald[3] attempts this by using turbulent flow correlations to link Direct Numerical Simulation work at the propellant surface to 1D ballistics parameters. Additionally, Rettenmaier and Heister[4] interpreted their new data to fit the Lenoir-Robillard model with a new coefficient, meant to reduce overprediction. However, as shown below, both these models drastically overpredict large-scale motors like RSRM.

II.   The Available Data

Besides the Furfaro Old 5-Inch CP Tandem data, a number of erosive burning test motors with real-time burn rate measurement at a broad range of conditions were tested by Strand, et. al.[5,6,7,8] at the Jet Propulsion Lab (JPL). The data from six of these are extant and clean enough to be useful for this study. Subsequently to the JPL and Old 5-Inch CP Tandem data, additional 5-inch CP Tandem motors were tested with RSRMV propellant, utilizing 7 segments per motor and 3 throat sizes[9]. By measuring propellant web thickness with ultrasonic gages, the burn rate was determined at cross-flow Mach numbers up to Mach 0.8. The available ultrasonic measurement system had 6 channels, so burning surface regression was measured at the first 3 and last 3 segments. Furthermore, the use of different throat sizes in otherwise identical motors provides a unique look at the effect of pressure and base burn rate on the erosive response. The data from lowest-Mach and highest-Mach motors of this test campaign have been added to that of Strand and Furfaro for this analysis.
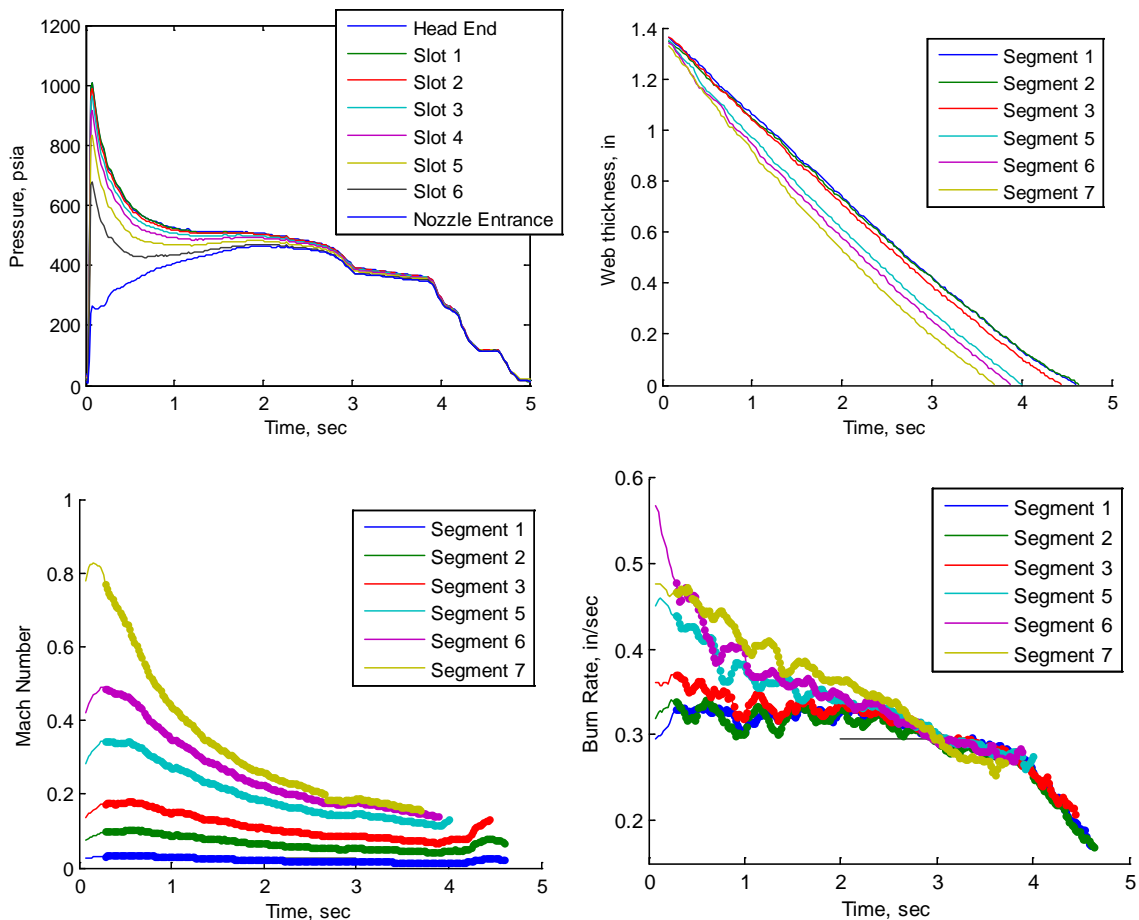

Figure 1. High Mach Test Motor Data: Measured Pressure and Web Thickness, Computed Mach Number and Burn Rate

American Institute of Aeronautics and Astronautics

Figure 1 shows an example of the data pertaining to the high Mach motor, where the port area is initially less than the throat area. Note that a clear erosive burning effect is apparent as late as 2 sec. The availability of so many measurements during quasi-steady operation obviates the need to account for ignition pressurization in the data analysis, as in Rettenmaier and Heister. Since differentiation of the web thickness data is required, the burn rate data was processed using a smoothing method developed to reduce the noise without too severely introducing end effects that limit the range of useful data. This smoothing method allowed the use of the lower-Mach motor data starting at 0.1 sec and the high-Mach motor data starting at 0.28 sec. Then, an empirical ballistics scheme was used to estimate the flow condition based on the burn rate and pressure measurements.

To correlate the segment midpoints ultrasonic regression data to the pressure data taken at each slot between segments, the pressure data must be processed to determine segment midpoint pressures. In the previous Furfaro work, it was found by Computational Fluid Dynamics (CFD) modeling that the average of the two measurements on either end of the segment was a good estimate of the pressure in the middle of the segment. Such work was repeated here, with the lower-Mach motor being modeled at 0.1 sec, and the high-Mach motor at 0.28 sec. For the low-Mach motor, the CFD-computed pressure at the middle of each segment was within 4 psi of the average of neighboring slot pressures, for less than 0.5% error. For the high-Mach motor, the errors were similarly low, except for the aft segment. However, as shown in Fig. 2, because of the difference in shape of the curve, near the end of the motor, it is difficult to surmise a better relationship. Thus, the midpoint pressure averaging method was used for the aft segment as well, but any resulting error only affects 3 out of 285 data points after processing.
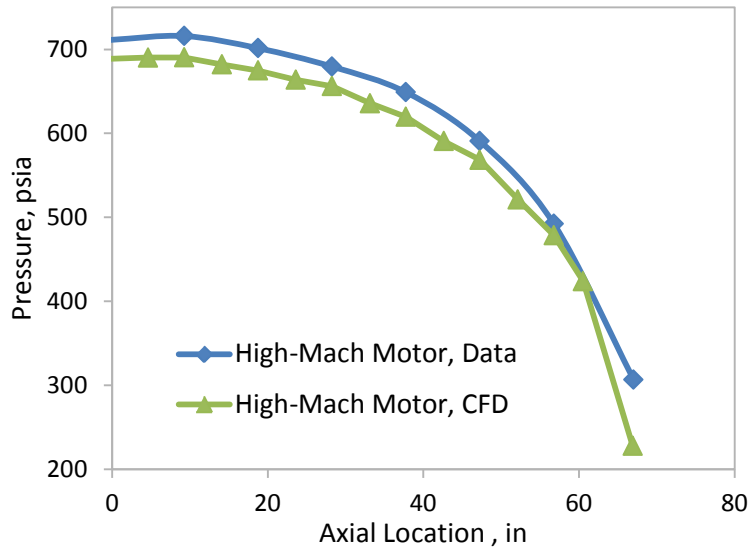

Figure 2. High-Mach Motor Pressure Measured and Modeled.

Figure 3 shows the impact of the differing range of test condition on the measurement results. In this limited case, mass flux appears more capable of predicting erosive burning at the different pressure conditions. However, the mass flux parameter does not include any information about motor scale, thus making it inadequate for building
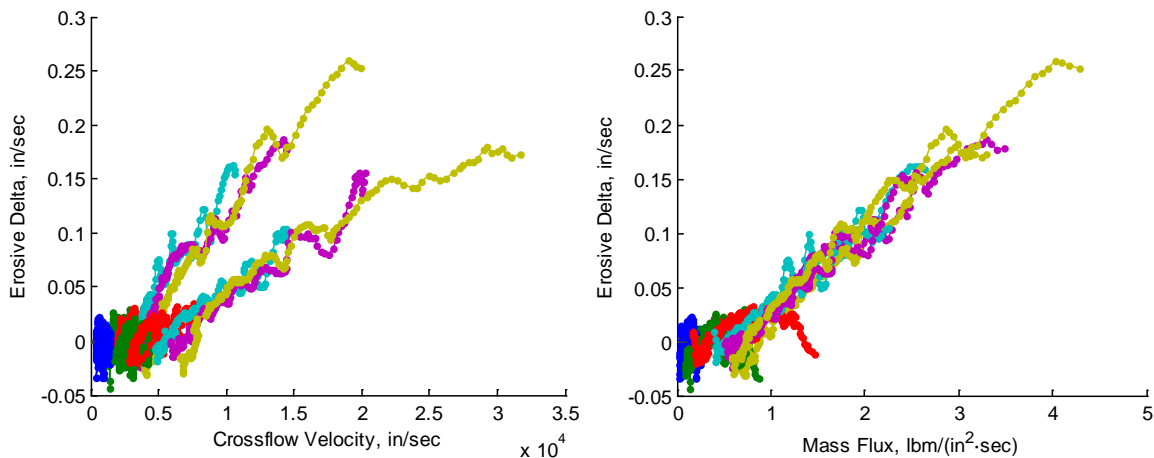

Figure 3. Erosive Contribution to Burn Rate United Better by Mass Flux for Two Motors

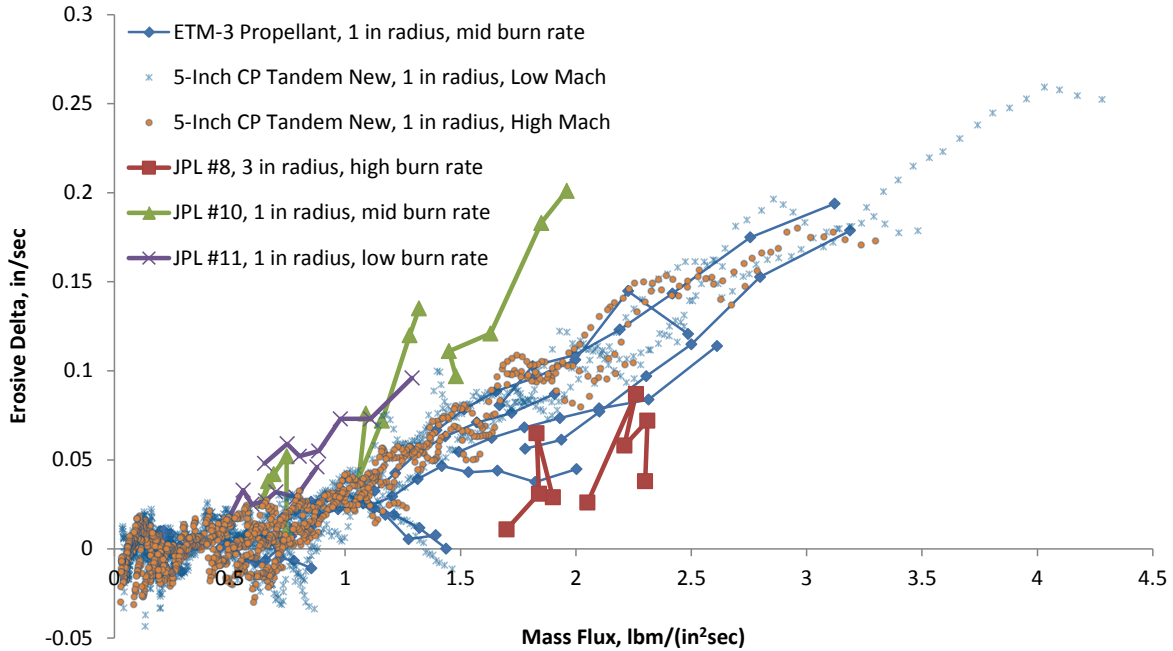American Institute of Aeronautics and Astronautics

Figure 4. Erosive Behavior of Similar Propellants From Different Test Series

a predictive model. After more data is added at multiple burn rates and scales, Fig. 4, its generality is further questioned.

Though some of the JPL motors were tested at different initial port diameters of 2, 4, and 6 inches, and the latest data spans a range from 2 to 4.8 inches diameter, these datasets alone are insufficient to characterize how erosive burning scales with diameter. Statistical conclusions may be helpful, but are not conclusive because it's not a designed experiment with pristine data, so effects may be confounded and important factors overlooked. This is especially true if one desires a model capable of predicting motors with initial diameters as high as 60 inches. Fluid flow theory and semi-empirical turbulent modeling are necessary to derive a suitable correlating parameter. Besides accounting for motor scale, such a theory should account for any effect of pressure and base burning rate, which most models have found to be contributing factors.

III. Derivation from Flow Theory

It has been proposed that erosive burning response can be directly related to shear stress[10]. McDonald[11] attempted this using the smooth-wall turbulent Prandtl equation to link one-dimensional velocity, U_{1D}, to shear velocity, thus incorporating the motor diameter through the Reynolds Number's appearance in the Prandtl equation. However, it is questionable how well the Prandtl equation, derived for smooth, non-blowing wall pipes, applies to solid rocket motor flow. As shown below, his model does not respond strongly enough to motor scale, over-predicting large motors' erosive burning.

Instead, this work explores a turbulent flow function based on blowing wall flows. The literature contains a couple of significant sets[12,13] of blowing wall flat-plate data, which demonstrate a similarity relationship between the ratio of friction coefficients with and without blowing, C_f and C_{f0}, respectively, and the blowing parameter, B_f. The blowing parameter is a function of flow condition and friction coefficient, as in Equation (1), where v_w is the velocity of flow entering at the wall.

$$B_f = \frac{v_w}{U_{1D}} \frac{1}{C_f/2} \tag{1}$$

The relationship above can be solved implicitly for both C_f/C_{f0} and B_f, once the data have been fit with a suitable curve. Because the effect on friction factor was presented as a ratio C_f/C_{f0}, it may be applicable to blowing wall pipe-like solid rocket flow, even though the data was obtained for blowing wall flat plate flow. The base C_{f0} should be drawn from pipe flow theory instead.

American Institute of Aeronautics and Astronautics

Though the Prandtl equation could be selected as the C_{f0} relationship, it appears that solid rocket flow has more to do with fully rough than fully smooth flow. It is reasonable to assume that dimensional roughness is on the order of large ammonium perchlorate (AP) particle size, as Gross and Beckstead[14] showed that flow heterogeneity is similar in scale to the AP particle driving it. Even assuming one-fourth of the AP size as the defining roughness level, solid rocket flow at any but the smallest velocities can be expected to be fully rough. For the range of Reynolds numbers of interest, Equation (2) is an adequate correlation to within 2%, where D is the diameter and k_s is the equivalent roughness. For now, k_s is evaluated as equal to the AP particle diameter, but could instead be considered some function of it if supported by data or analysis.

$$\frac{C_{f0}}{2} = \frac{1.325/8}{\left(ln\left(\frac{1}{3.7}\frac{k_S}{D}\right)\right)} \tag{2}$$

Figure 5 shows the few witnesses to the effect of blowing on turbulent friction coefficient. "Simpson Data" and the "Simpson Fit" were both listed in Simpson's thesis[12]. "PMK Fit of Data <5" is the correlation listed in Pimenta, Moffat and Kays[13], whose data span was only from 1 to 5 on the $1+B_f$ axis. The "Boardman/Lees" curve is Boardman[15] quoting a 1958 study by L. Lees, for $1+B_f$ values from 5 to 100. All three of these curve fits appear to be combinations of convenient non-dimensional parameters, not equations rigorously derived from the underlying fluid mechanics. Thus if a more useful convenient relationship could be found, it would be just as valid even in extrapolation, if (1) it is consistent with the data and its associated error, (2) it correctly predicts the extreme values, and (3) it is simple enough to solve for C_f and B_f to facilitate building a 1D ballistics correlation consistent with erosive burning data. For condition (2), at $1+B_f = 1$, there is no blowing, so the ratio C_f/C_{f0} must equal 1; as $1+B_f$ approaches ∞, there is no significant crossflow relative to the strong blowing, and C_f/C_{f0} approaches 0. A function that meets all three criteria is shown in Equation (3) and plotted in Fig. 5.
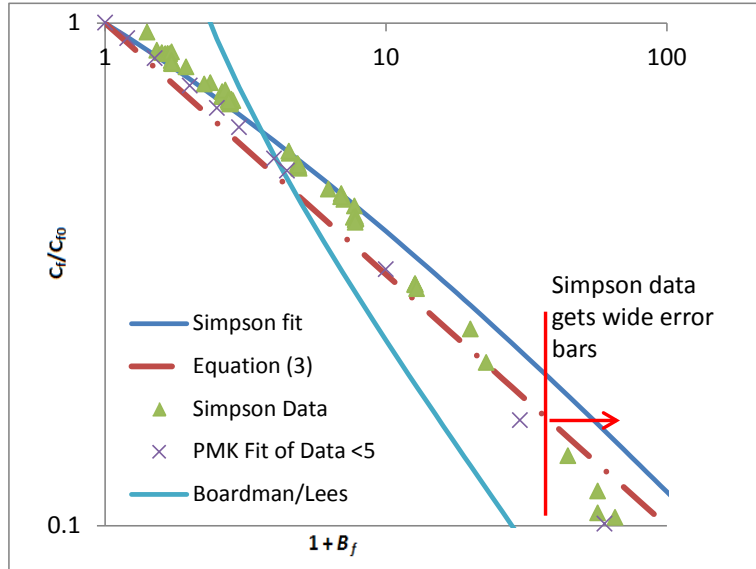

Figure 5. Blowing Wall Turbulence Results and Fits

$$\frac{C_f}{C_{f0}} = \frac{1}{\left(1+B_f\right)^{1/2}} \tag{3}$$

Combining Equations (1) and (3) allows solving for C_f explicitly in Equation (4).

$$\frac{C_f}{C_{f0}} = \frac{2}{\frac{v_w}{U_{1D}C_{f0}/2} + \sqrt{\left(\frac{v_w}{U_{1D}C_{f0}/2}\right)^2 + 4}} \tag{4}$$

Now the C_f can be calculated for every data point in the erosive burning test sets. Two related parameters appear potentially useful: the friction coefficient ratio itself, and the New McDonald Number, $NMcD$, defined in Equation (5). The New McDonald Number so called because it is equal in form to the square root of McDonald's Wall Momentum Ratio, except using shear stress based on Equations (2) and (4). This is shown for the two new motors in Fig. 6.

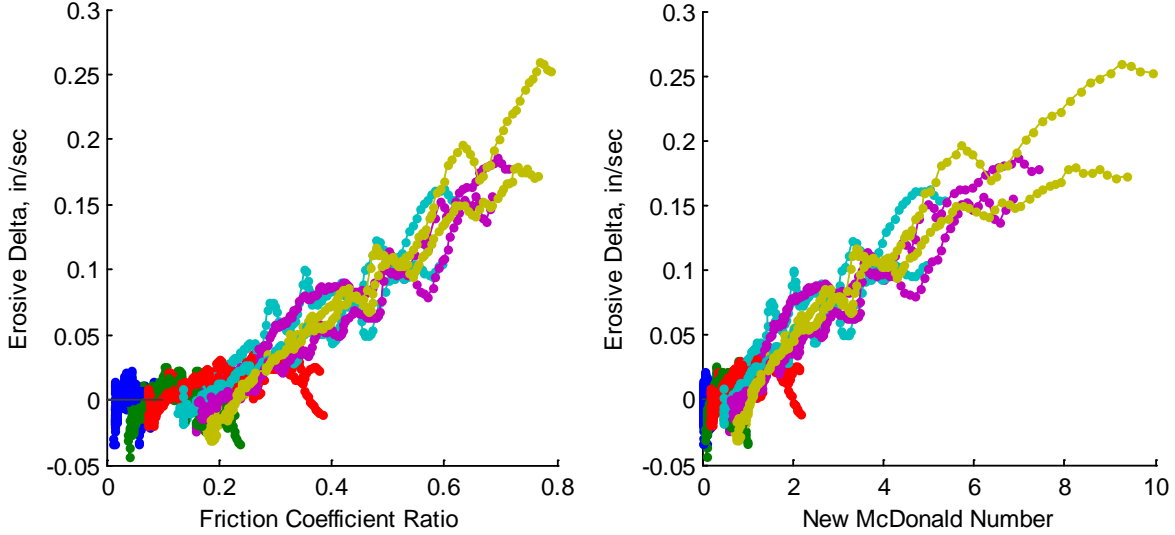$$NMcD = \sqrt{\frac{C_f}{2}} \frac{U_{1D}}{v_w} \tag{5}$$

Figure 6. Erosive Burning Correlates to Two Friction Coefficient Parameters

IV. Compilation of all the Data

Now it remains to empirically link the flow parameters to erosive burning level. In an attempt to balance the information gained from each of the three datasets available, further processing and selection of the data has been performed. Although the JPL dataset from Strand is the noisiest due to its microwave regression measurement technique, and provides the coarsest set of datapoints, it is important to allow it to affect correlations because it contains a higher range of port diameter and base burn rate than the other datasets. To put the 5-inch CP Tandem data on equal footing, the following three steps were performed:

1) Decimation. The data, originally 50 samples per second, were reduced to every 8th data point. This makes the change in web distance between data points comparable to that of the JPL data. As a part of this process, a 9-pt moving average smoothing was first performed, akin to anti-alias filtering.
2) Omission of points below the threshold. In order to get the data ready for linear fitting, only the data above the threshold must be used. The JPL data had already been thus truncated.
3) Omission of points after the first quarter of burn. The data show a clear Burn Anomaly Rate Factor (BARF) effect, where the non-erosive burn rate is affected as a function of web distance burned. BARF could skew the fit by having higher burn rate values from later times at lower flow conditions. To reduce that, only the first quarter of burn is used. This may be more fitting when using the model to predict anyway, because in full-scale motors the erosive burning would occur during the initial fraction of the burn. Although the JPL motors are not treated in the same way, any BARF effect would be obfuscated by the greater noise in the data.

This results in 83 JPL datapoints for 6 motors, 41 New 5-inch CP Tandem datapoints for 2 motors, and 163 Old 5-inch CP Tandem datapoints for 163 motors. This allows each dataset to have reasonable influence on line fitting and other statistical calculations.

First, the next several plots show the reduced data versus the various candidate independent variables. The three groups have been color-coded for now to maintain the distinctness for comparison. Notice first, in Fig. 7, the pros and cons of each candidate. The $(C_f/C_{f0})^2$ correlation on the left doesn't quite align the blue JPL data as nicely as the New McDonald Number on the right, but keeps the upper end of the range tighter and more linear. Both cases deliver a similar norm of residuals when line-fit, with the line rising from a positive threshold, where the threshold is at the same point in the data. Probably a useful correlation could be built on either choice of independent variable. The only theoretical consideration is that $(C_f/C_{f0})^2$ has an upper limit of 1, implying a maximum erosive burn rate. Whether the physics supports this has not been examined.
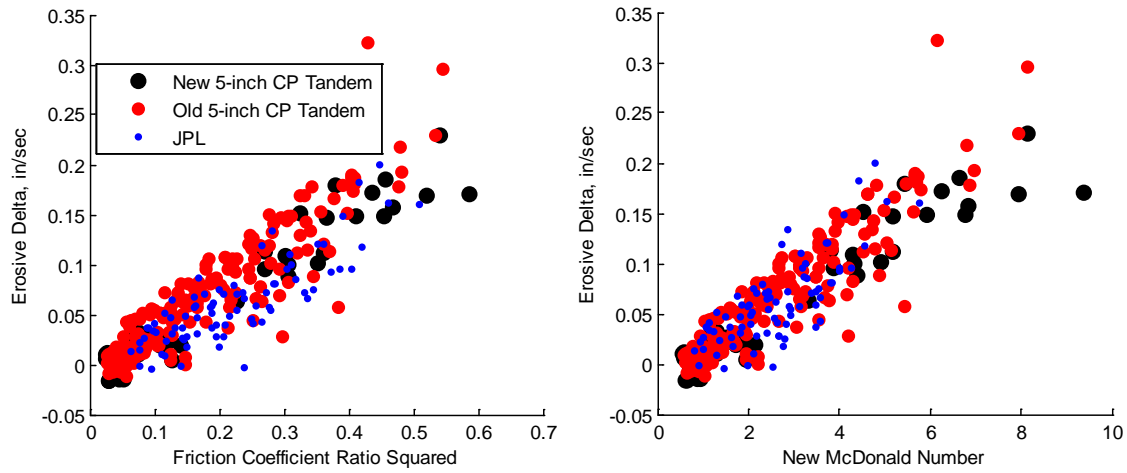
Figure 7. Combined Data as Correlated with Friction Coefficient Parameters
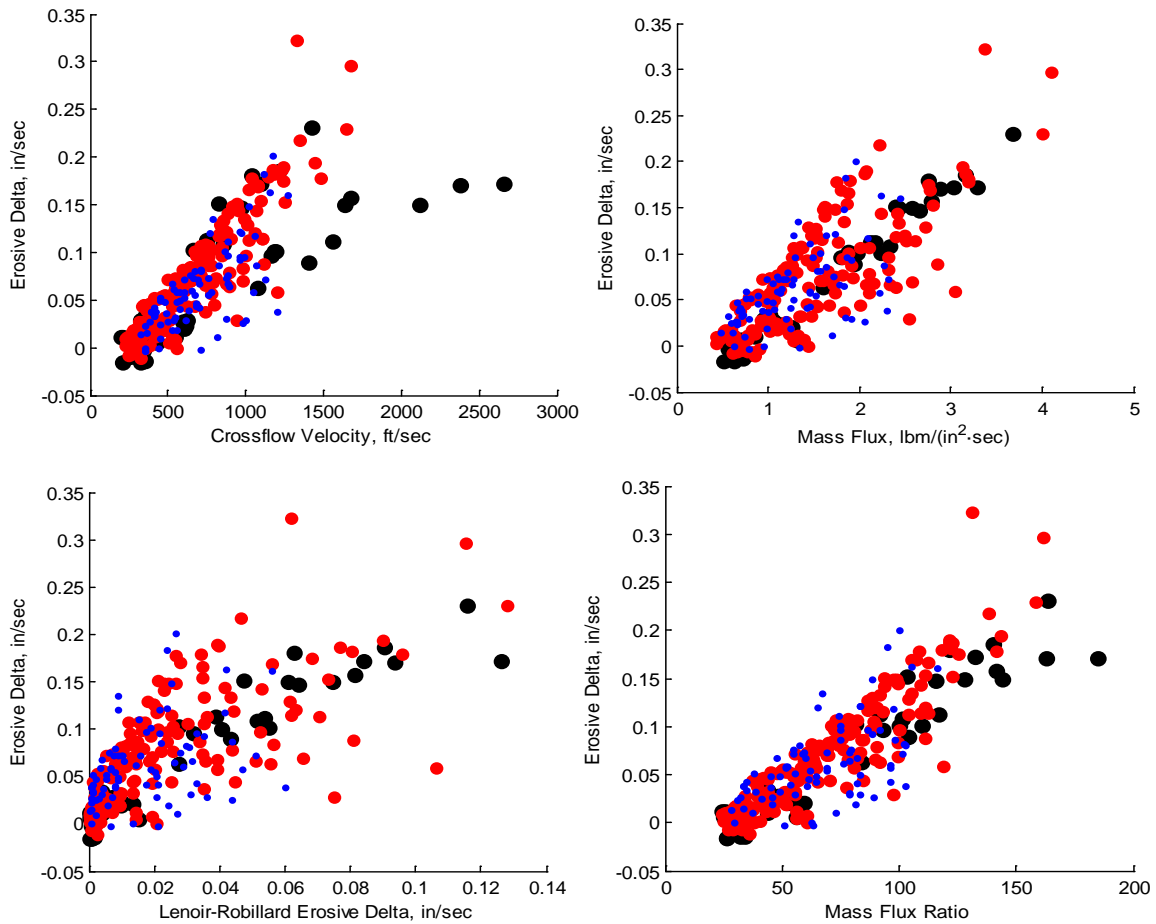

Figure 8. Combined Data Attempting to Correlate with Other Flow Parameters

Figure 8 shows alternate flow parameters. From the top row, it is clear that velocity and mass flux are ineffective across the various burn rates and pressure ranges represented by this data. The Lenoir-Robillard erosive burning difference, here computed with Rettenmaier's coefficients, is also not general enough to predict all the data. All these differences are not even primarily about motor scale, but mainly about the effect of base burning rate, pressure, or other propellant and flow parameters not being captured by the independent variable. The JPL dataset includes two motors with a 6-inch diameter initial port, but the rest of the motors had a 2-inch diameter initial port. Thus, in the Mass Flux Ratio plot, the spread of these blue points is a bit larger than in Fig. 7. While otherwise the Mass Flux Ratio appears similar in prediction quality, it will fail with large changes in motor diameter.

Figure 9. Ratio of Burn Rates Not as Good a Correlation

Another historic challenge in erosive burning model development is whether to let the burn rate difference or the burn rate ratio be the modeled dependent parameter. Figure 9 shows the ratio of total burn rate to base burn rate plotted against the New McDonald Number, where it is apparent that the data does not collapse to a single slope. Compare to Fig. 7, where a single slope is much more evident. Plotting the ratio against the other flow parameters suggests the same result.

Therefore, the desired dependent variable is burn rate difference, with the square of the Friction Coefficient Ratio and the New McDonald Number good options for the independent variable. These correlations are given in Equations (6) and (7), respectively, and shown in Figure 10. Other reasonable estimates of the correlating function could be found by using the confidence limits of the fitted function. Extrapolating to larger motors may indicate that a somewhat different slope and threshold are required, that still fit the underlying data well.

$$r_e - r_0 = \begin{cases} 0, & \left(\dfrac{c_f}{c_{f0}}\right)^2 < 0.02577 \\ 0.4036\left(\dfrac{c_f}{c_{f0}}\right)^2 - 0.0104, & \left(\dfrac{c_f}{c_{f0}}\right)^2 \geq 0.02577 \end{cases} \tag{6}$$

$$r_e - r_0 = \begin{cases} 0, & NMcD < 0.4928 \\ 0.03076\,NMcD - 0.01516, & NMcD \geq 0.4928 \end{cases} \tag{7}$$
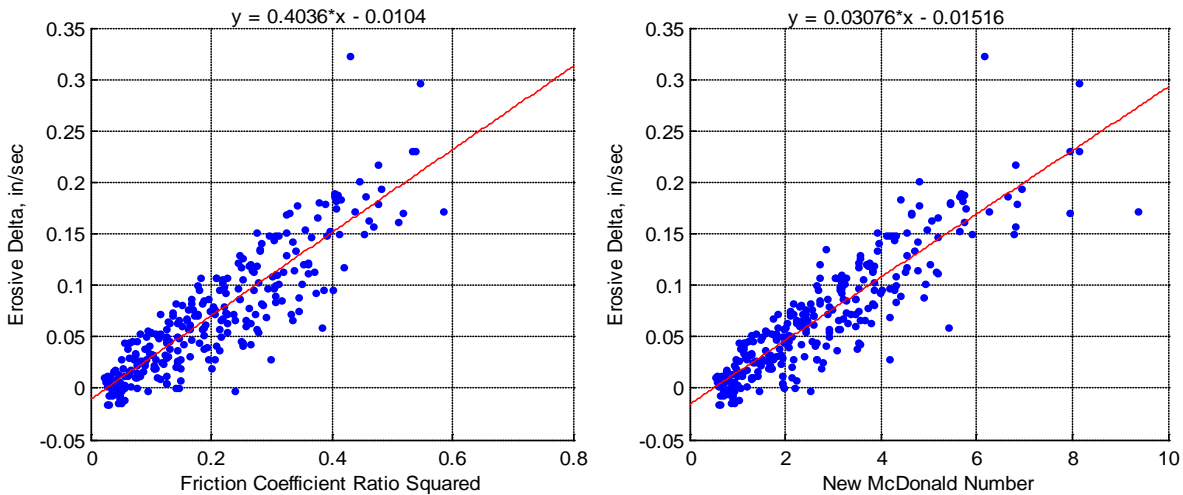

Figure 10. Correlation of All the Data with the Candidate Independent Variables

V. Preliminary Results in Large Motors

The performance of these models in large motors can be estimated. The RSRM and RSRMV are used for example, both motors having an initial port diameter of around 60 inches. A true ballistics analysis was not computed, because an appropriate tool has not yet been programmed. However, an initial estimate of the impact of erosive burning can be computed by the "open loop" method:

1) Compute the turbulent flow parameter from a standard 1D ballistics calculation output, at each axial station.
2) Use the correlating equations to compute the erosive burning difference, δr_e.
3) Compute the total additional mass flow rate due to δr_e.
4) Compute pressure increase as proportional to mass flow rate increase.

In reality, the additional mass due to δr_e would drive up the pressure more than linearly, because the pressure-dependent burn rate would also rise, and the geometry would also change. These effects are left for future work, knowing that the result would be a higher, but shorter duration, erosive burning effect.

Figure 11 and Figure 12 show the predicted erosive burning for the two models here, and two competing models. Distinctives of each series are:

1) Likely Range from Motor Data: This was done by subtracting two motor predictions for the first 25 sec from motor data. Because BARF adds an uncertainty of often 2-3% of absolute pressure, the effect of erosive burning cannot often be defined any more closely.
2) Friction Coefficient Ratio Squared: This is an open loop method calculation using Equation (6).
3) New McDonald Number: This is an open loop method calculation using Equation (7).
4) Lenoir-Robillard Model: This is a closed-loop, full ballistics prediction, using the Lenoir-Robillard Model and coefficients as presented by Rettenmaier and Heister.
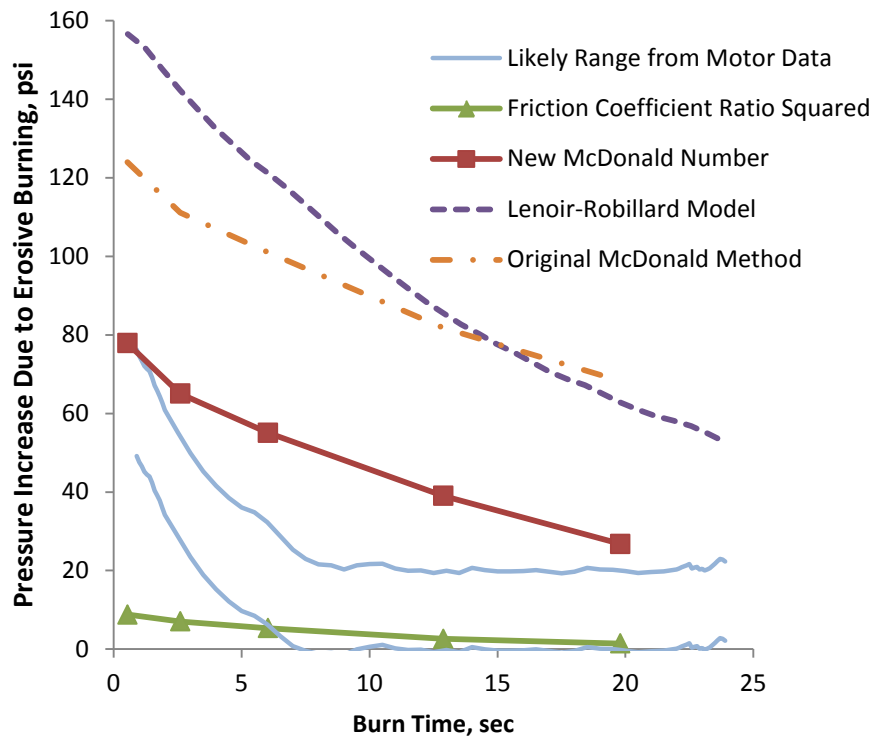5) Original McDonald Method: This is an open loop method calculation as implemented in the reference by McDonald.

Figure 11. RSRMV Erosive Burning Impact by Different Models

The two models presented herein scale up differently from the subscale to full-scale motors, with one predicting a bit too little, and one a bit too much erosive burning. However, both are much closer to the data than the Lenoir-Robillard or Original McDonald models. It is possible the two turbulent parameter models can be improved by:

1) Including an implicit correlation for blowing. The term v_w, as presently computed, is just the base burn rate without erosive burning times the ratio of gas to propellant densities. It may be more proper to use the total burn rate, including erosive burning.
2) Compute closed-loop ballistics prediction with the erosive burning models.
3) Try slopes and intercepts within the confidence limits of the data populations to see if the full-scale prediction is sensitive to such changes.
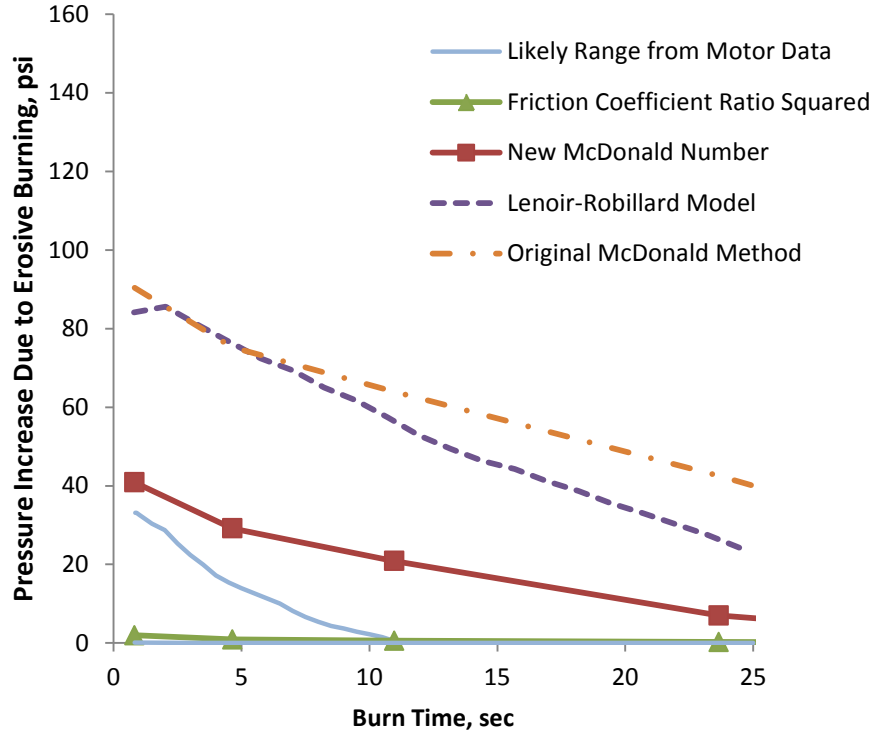

Figure 12. RSRM Erosive Burning Impact by Different Models

VI.   Conclusions and Further Work

The model candidates presented here are close to bridging the gap between data at 2 to 7 inches diameter and prediction at 60 inches diameter. The use of turbulent flow data and theory for blowing wall flow allows for motor scale inclusion without needing multi-dimensional CFD to set parameters for a 1D erosive burning model. Besides the three suggestions above for improving the models presented, further work should be undertaken in the following areas:
1) Study further the relationship between apparent roughness due to AP flame height, AP particle size, and pressure. Gross and Beckstead showed that pressure is a very significant factor for 400 micron AP, but not as significant for 50 micron AP.
2) Use these models to predict motors with non-axisymmetric grain shapes, like aft-end fin slots. Although not strictly applicable by the derivation, perhaps the results would turn out reasonable and useful, like when hydraulic diameter is used for pressure drop in non-circular ducts.
3) Derive a similarity formula for the turbulent velocity shape with blowing wall. It may be more accurate than the correlations herein, and might also work toward developing more accurate turbulence models for CFD in solid rocket motors.

Acknowledgments

References

[1]Landsbaum, E. M., "Erosive Burning of Solid Rocket Propellants-A Revisit," Journal of Propulsion and Power, Vol. 21, No. 3, 2005, pp. 470-477.

[2]Furfaro, J., "Real Time Erosive Burn Rate Evaluation Utilizing Ultrasonic Measurement Technique", Alliant Techsystems, ETP-1980, Brigham City, Sept. 2001.

[3]McDonald, B. A., "Numerical Analysis of the Correlation of Erosive Burning and the Threshold Condition in Solid Propellants Using the Wall Momentum Ratio," JANNAF Journal, Vol. 1, No. 1, 2008, pp. 17-27.

[4]Rettenmaier, A. K., and S. D. Heister, "Experimental Study of Erosive and Dynamic Burning in Polybutadiene-Based Composite Propellants," Journal of Propulsion and Power, Vol. 29, No. 1, January-February 2013, pp. 87-94.

[5]Strand, L., Yang, Y., Nguyen, M., and Cohen, N., "Erosive Burning Research," 22nd AIAA/ASME/SAE/ASEE Joint Propulsion Conference, AIAA-86-1449, June 1986.

[6]Strand, L., Nguyen, M., and Cohen, N., "The Scaling of the Threshold Conditions for Solid Propellant Erosive Burning," 24th AIAA/ASME/SAE/ASEE Joint Propulsion Conference, AIAA-88-3254, July 1988.

[7]Strand, L. and Cohen, N., "Erosive Burning Threshold Conditions in Solid Rocket Motors," 25th AIAA/ASME/SAE/ASEE Joint Propulsion Conference, AIAA-89-2528, July 1989.

[8]McComb, J. C., Behm, J. W., Hocutt, S. R., McKay, R. A., Rivkin, S. N., Strand, L. D., Compton, L. E., and Anderson, F. A., "ASRM Propellant Composition Tradeoff Study," Jet Propulsion Lab, JPL D-8765, Pasadena, 1991.

[9]Linke, K., Kibbey, T. P., and McMillin, J. E., "High Mach Number Erosive Burning Tests," ATK Launch Systems, Inc., ETP40200-A, Brigham City, 2008.

[10]Wang, Q,. "Development of Erosive Burning Models for CFD Predictions of Solid Rocket Motor Internal Environment," 39th AIAA/ASME/SAE/ASEE Joint Propulsion Conference and Exhibit, AIAA 2003-4809, July 2003.

[11]McDonald, B. A., "The Development of the Wall Momentum Erosive Burning Scaling Law and Macro Scale Erosive Burning Model," U.S. Army Aviation and Missile Research and Development Engineering Center, Technical Report RDMR-WD-10-15, Redstone Arsenal, AL, May 2010.

[12]Simpson, R. L., "The Turbulent Boundary Layer on a Porous Plate: An Experimental Study of the Fluid Dynamics with Injection and Suction," PhD Thesis, Stanford University, Stanford, CA, 1968.

[13]Pimenta, M. M., Moffat, R. J., and Kays, W. M., "The Turbulent Boundary Layer: An Experimental Study of the Transport of Momentum and Heat with the Effect of Roughness," Stanford University, Report No. HMT-21, Stanford, CA, May 1975.

[14]Gross, M. L., and Beckstead, M. W., "Steady-State Combustion Mechanisms of Ammonium Perchlorate Composite Propellants," Journal of Propulsion and Power, Vol. 27, No. 5, 2011, pp. 1064-1078.

[15]Sutton, G., *Rocket Propulsion Elements*, 7th ed., John Wiley & Sons, New York, 2001, Appendix 4, pp. 733-738.

American Institute of Aeronautics and Astronautics